Acta Crystallographica Section D
Biological Crystallography
ISSN 0907-4449

Crystallization and preliminary structural analysis of an antibody complex formed with PfMSP1-19, a malaria vaccine candidate

J. C. Pizarro, V. Chitarra, C. Calvet, D. Verger and G. A. Bentley*

Unité d'Immunologie Structurale, CNRS URA 2185, Institut Pasteur, 25 Rue du Dr Roux, 75724 Paris, France

Correspondence e-mail: bentley@pasteur.fr

Received 8 March 2002
Accepted 26 April 2002

The 11 kDa C-terminal fragment of the proteolyticly matured surface antigen, PfMSP1, from *Plasmodium falciparum* is a promising malaria vaccine candidate. The soluble recombinant form of this naturally occurring fragment has been crystallized as a complex with the Fab of a specific murine monoclonal antibody. The crystals belong to the space group $P2_1$, with unit-cell parameters a = 51.8, b = 213.5, c = 60.0 Å, β =101.0°, and with Z = 4. Diffraction data have been measured to 2.9 Å resolution and a preliminary model of the complex has been determined by molecular replacement. The epitope recognised by G17.12 is located on the N-terminal EGF-like domain of the antigen.

1. Introduction

Most efforts in the search for a malaria vaccine have been directed towards combating *Plasmodium falciparum*, the species responsible for most of the morbidity and mortality arising from the disease in man. Proteins exposed on the surface of the *Plasmodium* merozoite, the erythrocyte-invasive form of the parasite, are favoured candidates for vaccine development because they are prime targets of the humoral immune response from persons with naturally acquired immunity (Udhayakumar *et al.*, 1995; O'Donnell *et al.*, 2001). The most abundant surface protein of *P. falciparum* is merozoite surface protein 1 (PfMSP1), a 195 kDa molecule attached to the membrane by a glycosylphosphatidylinisotol (GPI) anchor (reviewed in Cooper, 1993). The protein undergoes two distinct proteolytic maturation steps. During the first step, which is thought to occur prior to release of the newly formed merozoites from the infected erythrocyte, PfMSP1 is cleaved into four well defined polypeptide fragments. These fragments remain associated as a non-covalent complex on the merozoite surface since the C-terminal 42 kDa product, PfMSP1-42, is fixed by the GPI anchor. The second proteolytic step takes place during or just prior to erythrocyte invasion: PfMSP1-42 is cleaved in two and the PfMSP1 polypeptide complex is shed, leaving only the C-terminal 11 kDa segment, PfMSP1-19, attached by the GPI moiety to the surface of the invading parasite. The second proteolytic step is essential for successful invasion since blocking this cleavage by specific monoclonal antibodies (mAb) or by serine-protease inhibitors prevents the merozoite from penetrating the erythrocyte (Blackman & Holder, 1991; Blackman *et al.*, 1994). Vaccination trials in animal-model systems have shown that immunization with PfMSP1-19 can lead to protective immunity (Egan *et al.*, 2000). These observations and the limited polymorphism present in this segment of PfMSP1 (less than 5% between different strains) have made the protein a leading vaccine candidate. The mechanisms of immune protection induced by PfMSP1-19 are still unclear, but different proposals have been put forward, such as the blocking of PfMSP1 processing mentioned above (Blackman *et al.*, 1994). In order to gain further understanding of the nature of the immune protection provided by the antigen and the role of the second proteolytic maturation step in erythrocyte invasion, we are engaged in structural studies of PfMSP1-19 and PfMSP1-42 and their complexes with specific monoclonal antibodies (mAbs). We report here the crystallization and preliminary structural analysis by molecular replacement of the complex formed between PfMSP1-19 and the Fab fragment of the murine monoclonal antibody G17.12.

2. Experimental

2.1. Preparation of Fab G17.12 and PfMSP1-19

PfMSP1-19 was cloned and soluble recombinant protein with a C-terminal hexahistidine tag was expressed in the baculovirus/insect cell system (S. Longacre, I. Holm & S. Pêtres, manuscript in preparation). The cell-culture supernatant was dialysed extensively and then applied to a metal-affinity column (Talon). After flushing out other proteins with a buffer containing 20 m*M* Tris pH 8.0 and 0.1 *M* NaCl,

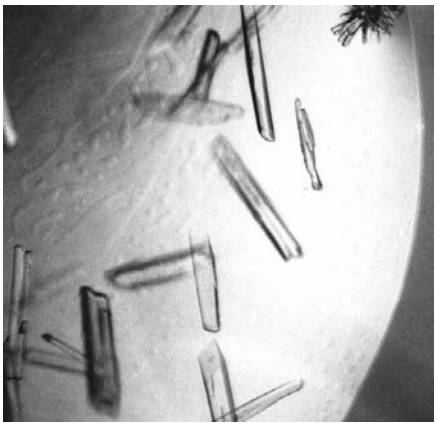

Figure 1
Crystals of the complex Fab G17.12–PfMSP1-19 grown by vapour diffusion.

PfMSP1-19 was eluted with 90 m*M* imidazole prepared in the same buffer.

The mAb G17.12 (isotype IgG2a, κ) was obtained by the hybridoma technique (Köhler & Milstein, 1975) after immunizing BALB/c mice with the soluble recombinant protein (S. Longacre, F. Nato & S. Dartevelle, manuscript in preparation). The IgG was precipitated from ascitic fluids using a saturated ammonium sulfate solution (pH 7.4) and purified by ion-exchange chromatography (DEAE-Sephacel, Pharmacia) using two steps of NaCl concentration (10 m*M* and 40 m*M*) in a phosphate buffer at pH 8.0. The purified antibody was dialysed against 0.1 *M* phosphate buffer pH 7.2 and concentrated in a Microprodicon tube. The IgG was then treated with papain in an enzyme:substrate ratio of 1:500 in the presence of EDTA (2.5 m*M*) and β-mercaptoethanol (3 m*M*) for 135 min, after which proteolysis was stopped by adding iodoacetamide (20 m*M*). The Fab G17.12 was separated from other proteolytic products, uncleaved IgG and papain by gel filtration followed by ion-exchange chromatography. It was subsequently concentrated in a Microprodicon tube.

2.2. Preparation of the Fab G17.12–PfMSP1-19 complex and crystallization

Recombinant PfMSP1-19 underwent significant non-specific aggregation (as evidenced by light adsorption at wavelengths higher than 320 n*M*), an effect that was aggravated at higher protein concentrations. The Fab complex was thus formed prior to concentrating the protein; after centrifuging to remove aggregated protein, the PfMSP1-19 solution (1.3 mg ml^{-1}) was added in a twofold stoichiometric excess over the Fab and left gently agitating overnight at room temperature. The resulting complex was purified by HPLC gel filtration and concentrated to 11 mg ml^{-1} in 10 m*M* Tris buffer at pH 7.4. No subsequent light absorption above 320 nm developed after complex formation, showing that sequestration by the Fab prevented PfMSP1-19 from undergoing further non-specific aggregation.

The search for crystallization conditions of the complex was performed using Crystal Screen solutions (Hampton Research). The final optimized crystallization buffer contained 0.075 *M* sodium acetate, 0.038 *M* sodium cacodylate, 11.3% PEG 8000 and 3% dioxane at pH 6.5. Crystals were grown by vapour diffusion at 291 K by suspending a drop comprising 3 µl of the concentrated protein solution and 3 µl of buffer over a 1 ml reservoir of buffer in a sealed environment. Optimal crystal growth was achieved within two weeks at 279 K, yielding specimens of up to 250 × 50 × 25 µm in size (Fig. 1). The crystals, however, were often multiple and separation of unique fragments was difficult.

2.3. Diffraction data measurements

Crystals were frozen in liquid nitrogen after a brief transfer to a cryoprotectant buffer (crystallization buffer with 15% glycerol) for diffraction measurements at cryogenic temperatures. The crystals belong to the space group $P2_1$ and have unit-cell parameters a = 51.8, b = 213.5, c = 60.0 Å, β = 101.0°. Data were collected on beamline ID14-1 (ESRF, Grenoble, France) using an X-ray wavelength of 0.934 Å. To minimize the effects of spot overlap on the diffraction images caused by the long b axis, crystals were screened in order to select for low mosaicity. Using a crystal with an estimated mosaic spread at 0.45°, a total of 360 images were recorded on a MAR CCD detector (MAR Research) with each image covering 0.5° rotation. The crystal dimensions were 0.30 × 0.05 × 0.02 mm. The crystal-to-detector distance was 240 mm and each image was exposed for 15 s. The crystal was translated in the beam halfway through the data collection in order to minimize the effects of radiation damage.

Diffraction data were integrated and scaled with the program package *HKL* (Otwinowski & Minor, 1997). A total of 27 530 unique reflections were measured in the 30–2.9 Å resolution range (redundancy = 3.39), with an overall $R_{\rm merge}$ of 0.071 and 96.8% completeness (0.578 and 87.6%, respectively, for the high-resolution shell between 3.0 and 2.9 Å resolution). Intensity statistics were analysed using the program *TRUNCATE* from the *CCP4* suite of programs (Collaborative Computational Project, Number 4, 1994); there were no indications of twinning but a high overall temperature factor of 86 Å^2 was indicated by the Wilson plot. The value of $\langle I/\sigma(I)\rangle$ is 16.5 for all data and 2.6 for the resolution range 3.0–2.9 Å. The value of $V_{\rm M}$, assuming two molecules in the asymmetric unit, is 2.8 Å^3 Da^{-1}, which falls within the range of observed values (Matthews, 1968) and corresponds to a solvent volume content of 56%.

3. Molecular-replacement analysis

A preliminary model of the crystal structure was determined by molecular replacement using the program *AMoRe* (Navaza, 1994), as implemented in the *CCP4* suite of programs (Collaborative Computational Project, Number 4, 1994). Rotation- and translation-function calculations were made using three independent search models corresponding to the different components that comprise the complex: a variable domain dimer (V_κ/V_H) and a constant domain dimer (C_κ/C_H1) for the Fab fragment and the homologous antigen from the

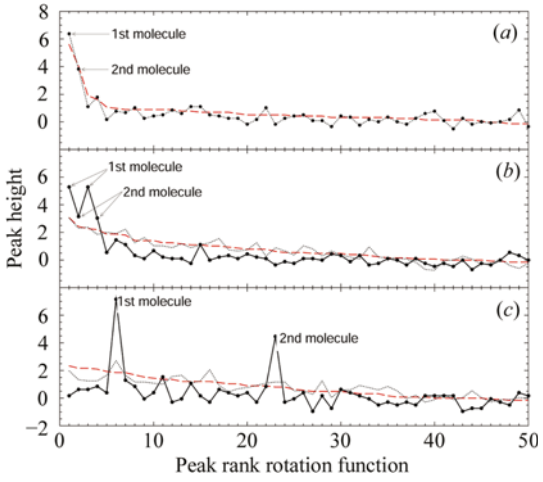

Figure 2
Peaks heights of the rotation-function and translation-function calculations plotted *versus* their rank in the rotation function. The units of the peak heights are described in the text. The rotation-function results are shown as red dashed lines, the single-body translation function is shown as black dotted lines and the multi-body translation search (see text) is shown as full black lines. (*a*) The variable dimer, (*b*) the constant dimer, (*c*) the antigen. The solutions for the two molecules of complex in the asymmetric unit are indicated for each search model.

species *P. cynomolgi* (taken from PDB entries 2igf, 1a3r and 1b9w, respectively). PfMSP1-19 has 45% sequence identity with the *P. cynomolgi* protein PcMSP1-19. The results of the analysis, which used all data in the resolution range 20–4 Å, are summarized in Fig. 2. For each search model, the top 99 solutions of the rotation function were taken for examination in translation searches. Peaks in the rotation and translation functions were normalized by first subtracting the mean peak height and then dividing by the root-mean-square deviation (r.m.s.d.). The clearest solutions were obtained with the variable dimer search (Fig. 2*a*). The rotation function gave two significant peaks at 5.6 and 4.0 r.m.s.d., respectively, above the mean (*c.f.* 1.8 r.m.s.d. for the third highest peak), consistent with two molecules of complex in the asymmetric unit. Both orientations gave a significant peak in the single-body translation search. These solutions were shown to be self-consistent when placed on a common crystallographic origin using a two-body translation search, thus confirming the validity of the result. By contrast, neither the constant dimer nor the antigen gave clear indications in the single-body translation searches. Their rotation-function peaks were therefore analysed by multi-body translation searches. A three-body translation search was performed for the constant dimer after placing the two variable dimers in the unit cell as indicated by the molecular-replacement results. The first four peaks of the rotation function gave the most significant peaks in the three-body translation search, with heights of 5.4, 3.0, 5.6 and 3.0 r.m.s.d., respectively (*c.f.* 1.5 r.m.s.d. for the next highest peak; see Fig. 2*b*). The first and third peaks were shown to correspond to the same solution since they converged to the same result when each was refined separately as a rigid body (initially separated by 3.03 Å r.m.s.d. in C^{α} positions, becoming 0.02 Å r.m.s.d. after refinement). Similarly, the second and fourth peaks, corresponding to solutions separated by 0.79 Å r.m.s.d. in their C^{α} positions, converged to the same result upon rigid-body refinement. We therefore conclude that in each case this was the effect of broad weak peaks in the rotation function rippled with noise, rather than the presence of two distinct conformations of the constant dimer. The two constant dimers thus selected gave structurally sensible pairings for the light and heavy chains of two Fab fragments when combined with the variable dimers and with no steric hindrance in the crystal packing. The translation function for the antigen was performed as a multi-body search with the two Fab molecules held fixed. This gave two very clear solutions from the sixth and 23rd rotation-function peaks (Fig. 2*c*), thus completing the crystal structure with two molecules of complex in the asymmetric unit. A rigid-body refinement gave a final correlation coefficient of 53.3% and an R value of 44.8% for all data in the 20–4 Å resolution range. The interactions between the Fab and the antigen in the model of the complex were identical for the two independent molecules in the asymmetric unit. Most intermolecular contacts between complexes are made by the variable domains and the antigen, with little participation from the constant domains. The constant domains could therefore have higher temperature factors, accounting for their weaker signal in the rotation and translation functions. Refinement of the structure at 2.9 Å resolution is in progress.

We thank the members of the ESRF staff for their help in taking diffraction measurements on beamline ID14, and Drs S. Longacre and F. Nato for scientific discussions and for providing material. This work received financial support from the European Union, Centre National de la Recherche Scientifique and the Pasteur Institute.

References

Blackman, M. J. & Holder, A. A. (1991). *Mol. Biochem. Parasitol.* **50**, 307–316.
Blackman, M. J., Scott-Finnigan, T., Shai, S. & Holder, A. A. (1994). *J. Exp. Med.* **180**, 389–393.
Collaborative Computational Project, Number 4 (1994). *Acta Cryst.* D**50**, 760–763.
Cooper, J. A. (1993). *Parasitol. Today*, **9**, 50–54.
Egan, A. F., Blackman, M. J. & Kaslow, D. C. (2000). *Infect. Immun.* **68**, 1418–1427.
Köhler & Milstein (1975). *Nature (London)* **256**, 495–497
Matthews, B. W. (1968). *J. Mol. Biol.* **33**, 491–497.
Navaza, J. (1994). *Acta Cryst.* A**50**, 157–163.
O'Donnell, R. A., Koning-Ward, T. F., Burt, R. A., Bockarie, M., Reeder, J. C., Cowman, A. F. & Crabb, B. S. (2001). *J. Exp. Med.* **193**, 1404–1412.
Otwinowski, Z. & Minor, W. (1997). *Methods Enzymol.* **276**, 307–326.
Udhayakumar, V., Anyona, D., Kariuki, S., Shi, Y. P., Bloland, P. B., Branch, O. H., Weiss, W., Nahlen, B. L., Kaslow, D. C. & Lal, A. A. (1995). *J. Immunol.* **154**, 6022–6030